Soft-phonon mediated structural phase transition in GeTe

Urszula D. Wdowik,[1] Krzysztof Parlinski,[2] Stéphane Rols,[3] and Tapan Chatterji[3]
[1]*Institute of Technology, Pedagogical University, Podchorążych 2, PL-30084 Kraków, Poland*
[2]*Institute of Nuclear Physics, Polish Academy of Sciences, Radzikowskiego 152, PL-31342 Kraków, Poland*
[3]*Institute Laue-Langevin, Boîte Postale 156, 38042 Grenoble Cedex 9, France*
(Received 18 March 2014; revised manuscript received 11 June 2014; published 30 June 2014)

Inelastic neutron scattering experiments on powder samples of GeTe together with density functional theory investigations of the phonon dynamics in the low- and high-temperature phases of GeTe crystal are reported. The dispersion of phonons in the high-temperature rocksalt phase show soft branches with the lowest one at the Γ high-symmetry point. The structural phase transition in GeTe is reconsidered and shown to be driven by the condensation of exactly three components of the triply degenerate optical transverse soft-phonon mode at the Brillouin zone center. The mechanism proposed allows us to explain the formation of structural distortions in the low-temperature ferroelectric phase of GeTe revealed by various experiments. A displacive nature of the phase change in crystalline GeTe is supported by the results of the present theoretical studies.

DOI: 10.1103/PhysRevB.89.224306 PACS number(s): 63.20.−e, 63.20.D−, 61.05.F−, 77.80.B−

I. INTRODUCTION

Germanium telluride has gained a renewed interest in the past few years not only because of its relationship with the phase-change materials $(GeTe)_m(Sb_2Te_3)_n$ (GST) applied in modern nonvolatile data storage devices [1], but also due to the physics underlying its properties, which are not yet fully understood. In particular, the nature of the phase transition [2,3] between its low-temperature ferroelectric rhombohedral $R3m$ structure (α-GeTe) and the high-temperature paraelectric rocksalt structure (β-GeTe) at $T_c = 650 \pm 100$ K is still a matter of controversy. A displacive versus order-disorder type of this transformation has been the subject of debate since the seminal works of Steigmeier *et al.* [2] and Chattopadhyay *et al.* [3]. The rocksalt-to-rhombohedral phase change was found to be accompanied by a relative shift of the Ge and Te sublattices (∼0.3 Å) along the original cubic cell diagonal and the reduction of crystal volume ∼1% [3,4]. Upon the atomic rearrangement, the crystal loses inversion symmetry, becomes noncentrosymmetric, and acquires a spontaneous polarization [5,6] along the threefold axis of the rhombohedral cell as large as ∼60 $\mu C/m^2$. A polar $R3m$ structure is also characterized by an angular distortion of ∼1.8° between the principal axes of the pseudocubic cell. A concurrent softening of the A_1 and E phonon modes with increasing temperature measured for α-GeTe by the Raman scattering experiments [2,7] as well as vanishing rhombohedral distortions above T_c observed in the neutron diffraction experiments [3] gave evidence for a displacive type of the structural phase transition in GeTe. Recently, however, x-ray absorption fine structure (EXAFS) experiments [8] and an analysis of the pair-distribution function [9] revealed the presence of the local structural lattice distortions, also frequently denoted as Peierls distortion [10], persisting above T_c in GeTe samples. Based upon this finding, a displacive type of the structural transition in GeTe was questioned, and the $R3m \rightleftharpoons Fm\bar{3}m$ transformation was suggested to be of an order-disorder type [8,9]. The misinterpretation of the displacive nature of phase transformation in GeTe was attributed to the intrinsic limitation/inability of the standard diffraction techniques to measure a local structure as they only probe the ensemble average structure, i.e., they are insensitive to random local distortions.

In recent years, not only experimental [11–19] but also theoretical works [5,6,20–22] have been undertaken to understand the electronic, dielectric, optical, and dynamical properties of the GeTe system at ambient conditions and under external pressure. Despite these efforts, the microscopic mechanism governing the phase change of GeTe still remains far from clear. The present work provides insight into the phonon dynamics of GeTe, which we gain from inelastic neutron scattering experiments performed on powder samples. We employ state-of-the-art density functional theory (DFT) together with a direct method to calculate phonons in the high- and low-symmetry phases of ideal (perfectly ordered and stoichiometric) GeTe crystal to reconsider the predominant character of the $R3m \rightleftharpoons Fm\bar{3}m$ structural phase transformation in this system.

II. METHODOLOGY

A. Experimental details

Inelastic neutron scattering measurements were performed on a GeTe powder sample (∼5 g) using the IN4C instrument, which is a time-of-flight spectrometer mounted on the thermal source at the Institut Laue Langevin (Grenoble, France). Incident neutrons with wavelengths 1.5 Å were used in elastic time-focusing conditions. This allowed us to study the (2–35 meV) energy range with ∼1.7 meV energy resolution [full width at half-maximum (FWHM)], by considering the downscattering (Stokes) side only. We performed another scan using a larger incident neutron wavelength of 2.4 Å in upscattering mode (for example, anti-Stokes scattering). In this mode, the maximum frequency attainable depends on the temperature of the sample. At 150 K, one can easily derive the phonon spectrum from ∼0.5 meV up to 50 meV providing the scattering of the sample is large enough. The unavoidable deterioration of the energy resolution with increasing energy transfer (resolution is 0.7 meV at elastic scattering, 1 meV at 10 meV, 1.4 meV at 20 meV, and 2.9 meV at 40 meV–FWHM) can be minimized by time focusing [23] in

the inelastic range, a condition requiring that the Fermi chopper spins at high speed. We chose a Fermi speed of 17 000 RPM and conditions so that frame overlap could be avoided.

The measurements were corrected for the scattering of the sample holder and normalized to vanadium. The signal was transformed into the so-called generalized density of states $G(E)$ in the framework of the incoherent approximation [24], after proper averaging of the scattered signal over the wide range of scattering angles (120°) provided by the IN4C multidetector.

Details of an analysis of neutron scattering data can be found elsewhere [25,26]. Here we mention that under the incoherent approximation, the neutron excitation spectrum of a powder sample averaged over a wide range of detector angles provides a direct measure of $G(E)$, defined as

$$G(E) = \sum_{\mu}^{N} c_{\mu} \frac{\sigma_{\mu}}{M_{\mu}} g_{\mu}(E), \qquad (1)$$

where the sum runs over all atoms in the unit cell, and c_{μ}, σ_{μ}, M_{μ}, and $g_{\mu}(E)$ are the concentration, total coherent scattering cross section, mass, and partial phonon density of states (contribution of atom μ to the phonon density of states), respectively, for the μth atomic species.

The room-temperature GeTe structure was characterized by neutron powder diffraction measurements performed on the time-of-flight powder diffractometer (POWGEN) located at the Spallation Neutron Source at Oak Ridge National Laboratory. The data were collected with neutrons of central wavelength 1.333 Å, covering a d-spacing range from 0.42 to 5.4 Å. Approximately 5 g of GeTe sample was loaded in a vanadium container of 10 mm diameter and was measured in the traditional ILL furnace at 300 K. The structure refinement was carried out using the FULLPROF suite [27].

B. Computational details

Calculations were performed within the DFT method using the VASP code [28]. Electron-ion interactions were described by pseudopotentials in the framework of the projector-augmented-wave (PAW) method [30]. Valence electrons of Ge and Te were described by the configurations ($4s^2 4p^2$) and ($5s^2 5p^4$), respectively. Gradient-corrected exchange-correlation functional in the form of GGA-PBE [29] and a plane-wave expansion up to 228 eV were applied. The rhombohedral and rocksalt unit cells of GeTe containing, respectively, two and eight atoms were sampled with the k-point meshes of $12 \times 12 \times 12$ and $10 \times 10 \times 10$ generated according to the scheme of Monkhorst and Pack.

Phonons were obtained within the harmonic approximation and using the direct method [31] based on the forces calculated via the Hellmann-Feynman theorem. The rocksalt and rhombohedral supercells of GeTe used to calculate phonons consisted of 64 and 128 atoms, respectively. The nonvanishing Hellmann-Feynman forces were generated by displacing the symmetry-inequivalent Ge and Te atoms from their equilibrium positions with the amplitude ±0.02 Å. The total number of calculated displacements amounted to 4 and 12 for the rocksalt and rhombohedral supercells, respectively. The phonon dispersions were computed through the diagonalization of the dynamical matrix $\boldsymbol{D}(\boldsymbol{k})$ for arbitrary wave vector $\boldsymbol{k}$, while the phonon density of states $g(\omega)$ was evaluated by sampling $\boldsymbol{D}(\boldsymbol{k})$ at fine gird of wave vectors.

GeTe is a semiconductor with a narrow gap [12] of the order of 0.1–0.2 eV resulting in the incomplete screening reflected by the Born effective charges carried by Ge and Te atoms. Hence, the long-range macroscopic electrostatic field accompanying atomic displacements splits the infrared-active (ir) phonon modes into the transverse optical (TO) and longitudinal optical (LO) components. In the direct method approach, the TO modes follow directly from the diagonalization of $\boldsymbol{D}(\boldsymbol{k})$, while the LO modes are determined by including a nonanalytic contribution [32] into $\boldsymbol{D}(\boldsymbol{k})$, which depends on the Born effective charge tensor $\boldsymbol{Z}^*$ and the electronic part of the dielectric constant $\boldsymbol{\varepsilon}^{\infty}$. Both $\boldsymbol{Z}^*$ and $\boldsymbol{\varepsilon}^{\infty}$ were calculated within the linear-response method [33] implemented in the VASP code.

Intensities of the Raman-active modes in the $R3m$ structure of GeTe were obtained [31] from derivatives of the electric polarizability tensor over the atomic displacements ($\partial \boldsymbol{\chi} / \partial \boldsymbol{u}$) [34]. The electric polarizabilities were calculated [28,33] for each symmetry-nonequivalent atom displaced from its equilibrium positions in the crystallographic unit cell by ±0.01 Å. Results are shown in the form of the Raman reduced spectrum $|\boldsymbol{g}_s\ \boldsymbol{\alpha}(j)\ \boldsymbol{g}_i|^2$, where $\boldsymbol{\alpha}(j) \sim \partial \boldsymbol{\chi} / \partial \boldsymbol{u}$ denotes the Raman susceptibility tensor of the jth phonon mode and $\boldsymbol{g}_i$ ($\boldsymbol{g}_s$) is the polarization versor of the incident (scattered) radiation.

III. RESULTS AND DISCUSSION

We start our considerations on the GeTe system from its fully optimized high-symmetry rocksalt structure, and we calculate the phonon-dispersion relations under the symmetry constraints of the space group $Fm\bar{3}m$. Figure 1 shows results of these calculations carried out for the lattice constant of 6.0116 Å, which remains in close agreement with that

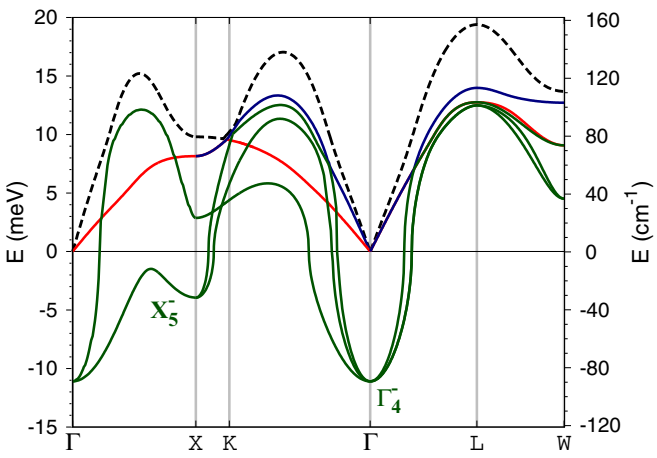

FIG. 1. (Color online) Phonon-dispersion relations for the rocksalt GeTe at the optimized lattice constant of 6.0116 Å. Transverse and longitudinal modes are marked by solid and dashed lines, respectively. Imaginary frequencies are denoted by negative values [$\omega^2(\mathbf{k}, j) < 0$]. The high symmetry points are labeled according to the Brillouin zone of the $Fm\bar{3}m$ space group. Note the degeneracy of transverse acoustic branches along the Γ-X-K and Γ-L paths.

measured above T_c (6.010–6.020 Å) [11]. At the ground state, the rocksalt phase of GeTe exhibits soft phonons at the Γ and X high-symmetry points. They are due to the TO components. Here, we do not take into account the dipole-dipole interaction being responsible for the LO-TO splitting when $\boldsymbol{k} \to 0$, i.e., near the Γ point, as we are interested mainly in the behavior of soft-phonon modes. These are the TO components that govern the symmetry changes at the phase transition [35]. Moreover, the nonanalytic term, which depends generally on the ratio $Z^*/\sqrt{\varepsilon_\infty}$, is strongly suppressed in the paraelectric rocksalt phase of GeTe due to enormously high dielectric constant (∼1000–2000) in the vicinity of the phase transition, as indicated by the recent experiments [18,19].

An irreducible representation of a given soft mode provides relationships between group and subgroup(s) together with a unit cell of a low-symmetry phase and mutual orientations of a parent and a daughter phase [36]. Furthermore, the polarization vector of the soft mode indicates directions of the atomic displacements, i.e., the distortions of the parent structure that lead to the low-symmetry structure [37,38]. The triply degenerate mode Γ_4^- with symmetry T_{1u}(TO) and frequency i 11.10 meV shows the strongest instability and can be responsible for the $Fm\bar{3}m \leftrightharpoons R3m$ transition. The $Fm\bar{3}m$ space group could be lowered by the irreducible representations of the soft mode Γ_4^- as follows [36]:

$$Fm\bar{3}m \to (\Gamma_4^-, e_1 \neq 0, e_2 = e_3 = 0) \to I4mm, \quad (2)$$

$$Fm\bar{3}m \to (\Gamma_4^-, e_1 = e_2 \neq 0, e_3 = 0) \to Imm2, \quad (3)$$

$$Fm\bar{3}m \to (\Gamma_4^-, e_1 = e_2 = e_3 \neq 0) \to R3m. \quad (4)$$

There is only one arm of the irreducible star of the three-dimensional Γ_4^- irreducible representation for the parent $Fm\bar{3}m$ group. Since the ray representation of Γ_4^- is three-dimensional, the order parameter consists of three components. In the first case, Eq. (2), one component of the Γ_4^- order parameter condenses, leading to the $I4mm$ space group, whereas in the second case, the condensation of two components of Γ_4^-, Eq. (3), results in $Imm2$ space group. Finally, one obtains the $R3m$ space group due to the condensation of three components, as indicated by Eq. (4). Two former paths of the symmetry lowering in the $Fm\bar{3}m$ space group [Eqs. (2) and (3)] do not lead to the $R3m$ phase, which is the stable structure of GeTe at low temperatures [2,3], and therefore they are not considered in the present work.

The soft-phonon mode X_5^- might induce transition from the paraelectric $Fm\bar{3}m$ phase to the ferroelectric $R3m$ phase [39], but in such a transition the resulting $R3m$ primitive unit cell would increase in size by a factor of 4 with respect to the size of the $Fm\bar{3}m$ primitive unit cell. This, however, would remain inconsistent with the experimental observations [2–4,40]. Moreover, the frequency of the X_5^- phonon (i 3.93 meV) is significantly higher than that of the soft-phonon mode Γ_4^-, and thus the soft X_5^- mode is not expected to drive the structural phase transition in GeTe.

The irreducible star of the wave vector $\mathbf{k}$ and the polarization vectors $\mathbf{e}(\mathbf{k}, j)$ of the soft mode components define the lattice distortions and atomic displacements generating the stable configuration. Indeed, the soft mode Γ_4^- with exactly three components condensed involves relative displacements of the Ge and Te sublattices along the [111] direction (cubic cell diagonal). We applied the systematic *frozen-phonon* calculations to look upon the energetically favorable $R3m$ structure of GeTe. They allowed us to establish a variation in the relative energy $\Delta E(Q)$ as a function of amplitude of the static unstable Γ_4^- mode with three components condensed according to Eq. (4). Results of these calculations are shown in Fig. 2. They indicate that the soft-phonon mode with the amplitude $Q_{\min} = 0.4235$ Å minimizes the system energy. The configuration $[Q_{\min}, \Delta E_{\min}(Q_{\min})]$ corresponds to the Ge-Te sublattice separation of $a_c\sqrt{3}u$ with $u_{\min} = 0.0305$ (0.321 Å). This stable $R3m$ structure is also characterized by $a_c = 6.0849$ Å and $\alpha_c = 88.11°$. A comparison of the calculated structural parameters with those measured at room temperature is provided in Table I. Results of the present measurements and calculations are consistent with most of the previous experiments [3,4,7,16,17].

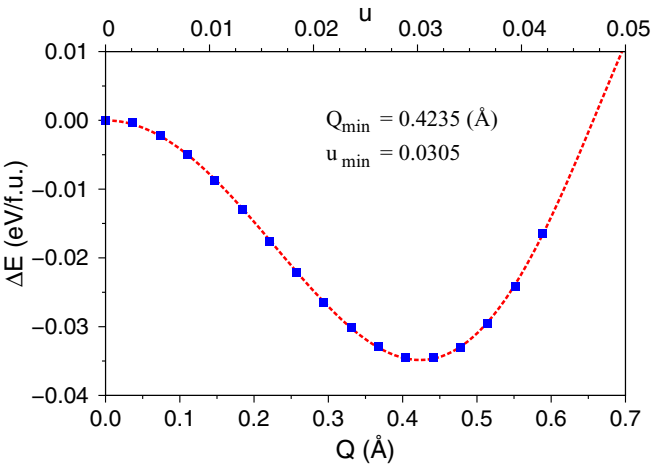

FIG. 2. (Color online) Change in relative energy (ΔE) as a function of amplitude of the frozen Γ_4^- mode (Q). The energy of the ideal rocksalt GeTe ($Fm\bar{3}m$ space group) is taken as the reference. Relative displacement of the Ge and Te sublattices (u) are denoted by the upper axis. The dashed curve corresponds to the polynomial fit $\Delta E = \frac{1}{2}aQ^2 + \frac{1}{4}bQ^4 + \frac{1}{6}cQ^6$.

The minimum-energy rhombohedral structure following from the condensation of triply degenerate Γ_4^- mode exhibits local distortions of Peierls type that result in three shorter (2.86 Å) and three longer (3.25 Å) bonds. The electronic origin of these distortions either in GeTe or the group-V semimetals has been widely discussed in the literature [21,22,41]. The current research shows that Peierls distorted GeTe is lower in energy than undistorted cubic GeTe by ∼35 meV per formula unit. Moreover, there is a pronounced increase in the system band gap while going from the undistorted rocksalt phase (0.26 eV) to the distorted rhombohedral one (0.48 eV). The GeTe phase with local distortions also reveals increased charge transfer from the Ge to the Te ion (0.414e) compared to GeTe with perfect sixfold coordination (0.393e), as indicated by the Bader charge analysis [42].

Phonon-dispersion relations calculated for the $R3m$ phase satisfying the configuration $[Q_{\min}, \Delta E_{\min}(Q_{\min})]$ are shown in Fig. 3. The LO-TO splitting follows from $\boldsymbol{Z^*}$ and $\boldsymbol{\varepsilon}^\infty$ calculated

TABLE I. Calculated and experimental structural parameters of α-GeTe. For convenience, the lattice parameters of the rhombohedral GeTe are expressed within the pseudocubic, hexagonal, and rhombohedral crystallographic representations of the $R3m$ space group.

	Theory	Experiment (309 K)
	Pseudocubic setting	
a_c (Å)	6.0849	5.9818
α_c (deg)	88.1100	88.2615
u	0.0305	0.0278
	Rhombohedral setting	
a_r (Å)	4.3730	4.2934
α_r (deg)	57.8642	58.0321
x	0.2347	0.2361
	Hexagonal setting	
a_h (Å)	4.2311	4.1651
c_h (Å)	10.8814	10.6704
x	0.2347	0.2361

for the configuration $[Q_{\min}, \Delta E_{\min}(Q_{\min})]$. In the $R3m$ phase, both $\boldsymbol{Z}^*$ and $\boldsymbol{\varepsilon}^\infty$ tensors are diagonal and consist of two independent components that are perpendicular and parallel to the threefold rotational axis, i.e., $(Z^*_\perp, Z^*_\parallel)$ and $(\varepsilon^\infty_\perp, \varepsilon^\infty_\parallel)$. The calculated $\boldsymbol{Z}^*(5.38, 3.01)$ and $\boldsymbol{\varepsilon}^\infty(38.05, 34.48)$ indicate that the components of $\boldsymbol{Z}^*$ and $\boldsymbol{\varepsilon}^\infty$ along the threefold axis are smaller than the components perpendicular to this axis. A similar effect has already been reported in previous DFT studies [6], although much larger values of $\boldsymbol{\varepsilon}^\infty$ components have been obtained. The present calculations yield the averaged $\langle\varepsilon^\infty\rangle = 36.86$, which lies in the range of 34–37.5, predicted by reflectivity measurements [13].

Phonons at the zone center of the rhombohedral GeTe crystal can be classified according to the irreducible representation of the point group C_{3v}. For this phase, the group theory predicts the modes with symmetries of A_1 and E that are both Raman- and infrared-active due to the lack of inversion symmetry. The A_1 is a nondegenerate mode, while the mode E remains doubly degenerate. The modes A_1 and E arise from vibrations of the Ge and Te sublattices along and perpendicular to the threefold axis, respectively. The phonons of symmetry E split into transverse (E^T) and longitudinal (E^L) components along the x-Γ direction, i.e., in the xy basal plane perpendicular to the threefold axis, whereas they remain doubly degenerate along the Γ-T direction, which denotes the direction parallel to the threefold axis. The optical branch due to the transverse A_1^T phonon is observed in the x-Γ direction, but its longitudinal component (A_1^L) is seen along the Γ-T direction. According to the selection rules, the Raman scattering configuration $Z(XX)\bar{Z}$ enables us to observe the E^T and A_1^L modes simultaneously, while the Raman setting $Z(XY)\bar{Z}$ selects the pure E^T mode [see Fig. 4(a)]. One expects an appearance of the pure A_1^T mode and a combination of the A_1^T and E^L modes at $X(ZZ)Y$ and $X(YY)\bar{X}$ scattering configurations, respectively. The Raman spectrum of polycrystalline GeTe simulated in backscattering

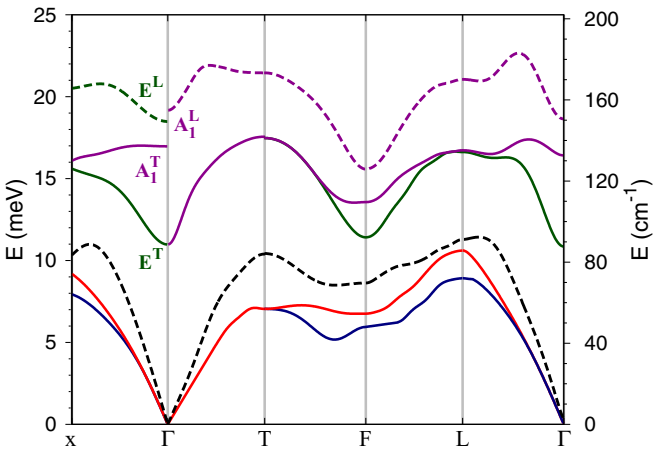

FIG. 3. (Color online) Phonon-dispersion relations for the rhombohedral GeTe at the lattice parameters satisfying the configuration $[Q_{\min}, \Delta E_{\min}(Q_{\min})]$. Transverse and longitudinal modes are marked by solid and dashed lines, respectively. The high symmetry points $x(-\frac{1}{3}, \frac{1}{6}, \frac{1}{6})$, $T \equiv Z(\frac{1}{2}, \frac{1}{2}, \frac{1}{2})$, $F(0, \frac{1}{2}, \frac{1}{2})$, and $L(\frac{1}{2}, 0, 0)$ are labeled according to the Brillouin zone of the $R3m$ space group. The TO and LO modes are denoted by superscripts T and L, respectively.

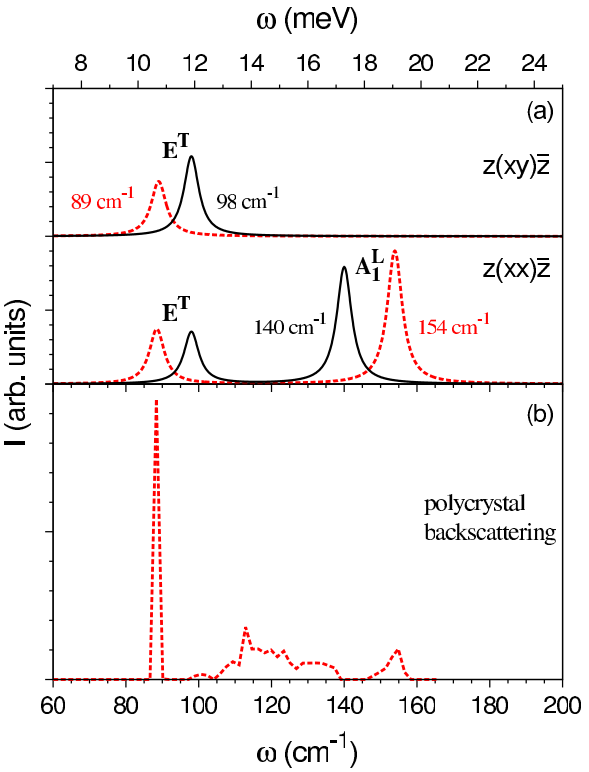

FIG. 4. (Color online) (a) Comparison of the experimental [2] (solid lines) and calculated (dashed lines) Raman spectra for rhombohedral GeTe crystal at scattering geometries $Z(XX)\bar{Z}$ and $Z(XY)\bar{Z}$. Theoretical peaks are represented by a Lorentzian with experimental HWHMs and intensities calculated at the following experimental conditions: $T = 82$ K and a He-Ne laser beam of 632.8 nm wavelength. For clarity, experimental HWHMs of peaks ($\sim$20 cm^{-1}) were artificially reduced to 2.5 cm^{-1}. (b) Simulated Raman spectrum of a polycrystalline sample in backscattering geometry.

geometry [see Fig. 4(b)] is dominated by the sharp, intense E^T mode separated from a low-intensity band of frequencies arising from TO and LO modes. Such a broad frequency distribution is expected in a polycrystal since the change in the frequencies of modes with orientation of crystalline grains would smear out the Raman peaks.

The present calculations yield the following frequencies of phonons at the Γ point: $E^T(89\ \mathrm{cm}^{-1})$, $A_1^T(137\ \mathrm{cm}^{-1})$, $E_1^L(149\ \mathrm{cm}^{-1})$, and $A_1^L(154\ \mathrm{cm}^{-1})$. The frequency of the E^T mode seems to be predicted in closer agreement with the results of experiments [2,7] (85–98 cm^{-1}), while the frequency of the A_1^L phonon is much more discrepant from its experimental value of 130–140 cm^{-1}. Significant overestimation of the theoretical A_1^L mode frequency has already been pointed out by Shaltaf *et al.* [6]. It should be noted that GeTe is a nonstoichiometric compound with quite a high concentration of free charge carriers ($\sim 10^{20}$–10^{21} cm^{-3}) arising from the presence of about 1–2 at. % Ge vacancies [12–15]. In fact, our DFT calculations performed for the rhombohedral $Ge_{1-x}Te$ crystal with $x = 1.6\%$ ($\sim 10^{21}$ holes/cm^3) show that these defects drive the GeTe system to a metallic state [43]. In this case, the long-range dipole-dipole interaction is completely screened by free charge carries, which is equivalent to the removed nonanalytic correction term in $\boldsymbol{D}(\boldsymbol{k})$ and results in $A_1^L \equiv A_1^T$ at $\boldsymbol{k} \to 0$. One notes that the calculated frequency of the A_1^T mode (137 cm^{-1}) is closer to the frequency of the A_1^L mode determined in a variety of the Raman spectroscopy experiments. Moreover, the screening effects of the long-range dipole-dipole interaction by free carriers may also account for the assignment of the A_1^L phonon to the frequency range of TO modes, as suggested by the early Raman investigations on GeTe crystals [2].

Experimental studies [2,7] show that both E^T and A_1^L modes decrease their frequencies with increased temperature, albeit with different rates. The A_1^L phonon mode was observed to soften more rapidly than the phonon mode of E^T symmetry. Finally, both modes converge into the triply degenerate mode of T_{1u} symmetry at the onset of the ferroelectric-to-paraelectric phase transition. A disappearance of these modes at T_c yielded a spectroscopic signature of the $R3m \rightleftharpoons Fm\bar{3}m$ phase transformation in GeTe as the rocksalt phase of GeTe remains Raman-inactive. The present simulations allow us to follow the behavior of the phonon modes upon the change in the amplitude of the frozen soft mode Γ_4^-. A gradual declining in the energies of E^T and A_1^L phonons with decreasing Q is observed up to the critical $Q_c = 0.29$ Å. The Q_c corresponds to the relative displacements between Ge and Te sublattices $u = 0.02$ (0.22 Å) and the angular distortion of $\sim 1^\circ$. For all amplitudes satisfying relations $Q < Q_c$, both E^T and A_1^L modes become soft. Structural distortions that progressively decrease with lowering Q affect also the phonons outside the Brillouin zone center. The most pronounced change in the phonon energy is encountered at the T point, where the frequencies of the acoustic phonons are imaginary at $Q < Q_c$.

Vibrational modes of the rhombohedral GeTe gather into three bands, as displayed in Fig. 3. They correspond to the acoustic, TO, and LO phonons. The acoustic band extends from 0 to ~11 meV. These features are also revealed by the generalized phonon density of states depicted in Fig. 5. In fact, the $G(E)$ spectrum differs from the *bare* phonon density

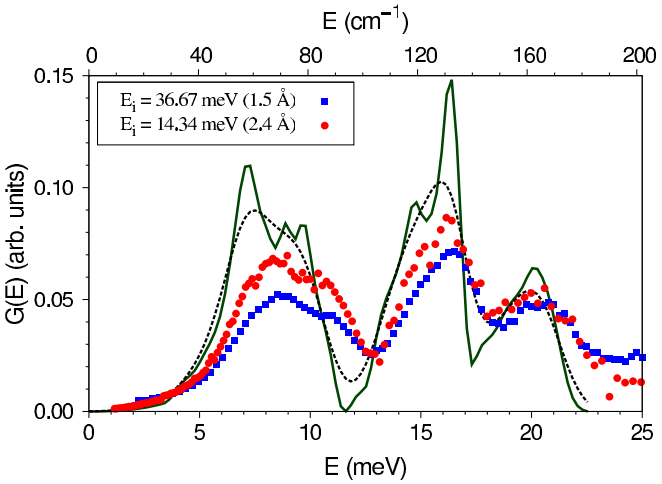

FIG. 5. (Color online) Generalized phonon density of states for rhombohedral GeTe measured at 150 K (symbols) for two incident neutron energies E_i and calculated at the ground state (solid line). The dashed line denotes the Gaussian convolution of theoretical $G(E)$ with the experimental resolution of 1.7 meV. Experimental and calculated $G(E)$ are normalized to unity.

of states by the weighting factors $c\,\sigma/M$ associated with the constituent elements [see Eq. (1)]. In the case of GeTe, the Ge atoms scatter with more than three times higher efficiency (0.118 barn/a.m.u.) than the Te atoms (0.034 barn/a.m.u.), and therefore the neutron-weighted density of phonon states is more sensitive to phonons involving motions of the Ge sublattice, which contributes ~78% to the $G(E)$ spectrum. Hence, the generalized phonon density of states can be directly compared to the partial density of states of the Ge sublattice. Both the experimental and calculated $G(E)$ spectra clearly indicate that the highest frequency region, which is due to the LO-phonon band, is dominated by the vibrations of the Ge sublattice. This is also validated by the calculated partial densities of phonon states as well as the ^{125}Te nuclear inelastic scattering experiments [17] performed on polycrystalline samples of GeTe, the latter sensitive to the dynamics of the Te sublattice. On the one hand, both TO and acoustic phonon bands involve mixed vibrations of the Ge and Te sublattices, but on the other hand, the spectral contribution to the TO band arising from motions of Te atoms along the threefold axis is strongly suppressed compared to the remaining contributions.

In general, there are two types of structural phase transitions driven by the soft-phonon mode and transforming the high-symmetry phase into the low-symmetry one, namely displacive and order-disorder. These two states can be distinguished based on a local atomic potential barrier [44]. In a displacive state, the local atomic potential barrier is very low or almost vanished, i.e., the potential energy of the collective atomic displacements has a single local minimum, in which atoms move very rapidly (with frequencies of the order of phonon frequencies). On the contrary, a disordered state is characterized by the local potential barrier with finite amplitude, and atoms perform jumps over the barrier between the local potential minima within much longer intervals, so they move in a multiwell local potential, i.e., they occupy

only a single local minimum. The present DFT calculations of the lattice vibrations in germanium telluride can provide information on whether the local atomic potential is single or multiwell, and hence they can verify the nature of the $Fm\bar{3}m \rightleftharpoons R3m$ phase transition in monocrystalline GeTe. Our identification is based on the analysis of values of the on-site force constant $\Phi_{ii}(\mu)$ for a given atom μ, which describes the curvature of the local potential barrier. Negative values of $\Phi_{ii}(\mu)$ for any atom correspond to local atomic potential of a multiwell-type, i.e., the local atomic potential barrier has a finite height and the crystal is stabilized by the anharmonic part of the interaction potential, while all positive values of $\Phi_{ii}(\mu)$ indicate that the local potential of a given atom has a single minimum, i.e., there is no local potential barrier between two states [44]. An example of the order-disorder phase transformation is the paraelectric-to-ferroelectric phase transition in $LiNbO_3$ [35]. In the paraelectric $LiNbO_3$, the Φ_{zz}(Li) is negative, whereas the remaining on-site force constant for Li, Nb, and O ions is positive. Hence, all local potentials have a single-well form except the local potential for Li ions along the z direction, which is represented by a double-minimum curve, which indicates that the phase transition in $LiNbO_3$ is of the order-disorder type. On the other hand, similar analysis applied to the phase transitions in perovskite-like $MgSiO_3$ and $CaTiO_3$ crystals revealed the displacive character of the high-temperature parent phases of these oxides [37,38].

Our calculations show that the on-site force constants of the Ge and Te atoms in the $Fm\bar{3}m$ phase are positive and amount to $\Phi_{xx}(\mathrm{Ge}) = \Phi_{yy}(\mathrm{Ge}) = \Phi_{zz}(\mathrm{Ge}) = +30.141$ N/m and $\Phi_{xx}(\mathrm{Te}) = \Phi_{yy}(\mathrm{Te}) = \Phi_{zz}(\mathrm{Te}) = +53.974$ N/m. This implies that the local potentials of both Ge and Te atoms have single minima, and it confirms the displacive nature of the structural transition in crystalline GeTe. We also note that the acoustic branches in the rocksalt phase of GeTe are positive close to $\mathbf{k} \rightarrow 0$, which indicates the mechanical stability of this phase above T_c. We should mention that at sufficiently large displacive amplitudes, atoms are affected by anharmonic terms that can stabilize the soft modes. Thus, anharmonicity and thermal fluctuations can be additional factors stabilizing the high-temperature rocksalt phase of GeTe above T_c. Nevertheless, the anharmonic effects have not been considered in the present work.

IV. SUMMARY AND CONCLUSIONS

The dynamical properties of GeTe, the parent compound of the phase-change materials, have been revisited by inelastic neutron scattering experiments and the phonon calculations based on density functional theory. These studies have been undertaken to gain better insight into the microscopic mechanism underlying the structural phase transition in GeTe, and to resolve whether the transition from its high-temperature rocksalt phase to the low-temperature rhombohedral phase is of a displacive or order-disorder type. The microscopic information available from our theoretical investigations together with symmetry arguments allowed us to establish a role of the Γ_4^- phonon in the $Fm\bar{3}m \rightleftharpoons R3m$ phase transition. This is the triply degenerate unstable TO mode at the zone center that freezes in to yield the stable ferroelectric rhombohedral phase at the ground state. The low-temperature structure of GeTe measured in the current inelastic neutron scattering experiments is shown to be a result of the condensation of exactly three components of the triply degenerate soft mode Γ_4^-. This mode, when condensed, produces rhombohedral distortions in the GeTe lattice, destroys the center of symmetry in the structure, and induces polarization along the trigonal axis. We note that electronic and vibrational properties of the GeTe lattice may remain very sensitive to such defects as Ge vacancies that induce free charge carriers in this system. The results of the current research indicate that both the low- and high-temperature phases of GeTe undergo an insulator-to-metal transition upon Ge vacancy incorporation. Hence, the long-range electrostatic interaction, responsible for the LO-TO splitting, can be strongly suppressed in *real* GeTe samples containing point defects. The $Fm\bar{3}m \rightleftharpoons R3m$ phase transformation in the defect-free, perfectly ordered, and single-domain GeTe crystal is displacive in origin as evidenced from a simple analysis of the atomic force constant values. One needs, however, to point out that nanodomain and local defect structures that are notably present in polycrystalline GeTe films can affect the character of the phase transition in this compound. This is somehow revealed by a significant spread in the transition temperature (± 100 K), which was found to be dependent on the actual sample composition [3]. Therefore, the nanoscale local structural distortions observed in polycrystalline GeTe films [8] at high temperature can reflect the internal morphology of samples used in experiments.

ACKNOWLEDGMENTS

We thank C. M. N Kumar, Forschungszentrum Jülich, Germany for his support during the diffraction measurements, and P. Piekarz, Institute of Nuclear Physics, Polish Academy of Sciences, Cracow, Poland for stimulating discussions. Interdisciplinary Center for Mathematical and Computational Modeling (ICM), Warsaw University, Poland and the IT4Innovations National Supercomputing Center, VSB-Technical University, Ostrava, Czech Republic are acknowledged for providing the computer facilities under Grant No. G28-12 and Reg. No. CZ.1.05/1.1.00/02.0070.

[1] M. Wuttig and M. Yamada, Nat. Mater. **8**, 824 (2007); J. Synder and E. S. Toberer, *ibid.* **7**, 105 (2008); G. I. Meijer, Science **319**, 1625 (2008).

[2] E. Steigmeier and G. Harbeke, Solid State Commun. **8**, 1275 (1970).

[3] T. Chattopadhyay, J. Boucherle, and H. G. von Schnering, J. Phys. C **20**, 1431 (1987).

[4] J. Goldak, C. S. Barret, D. Innes, and W. Youdelis, J. Chem. Phys. **44**, 3323 (1966).

[5] A. Ciucivara, B. R. Sahu, and L. Kleinman, Phys. Rev. B **73**, 214105 (2006).

[6] R. Shaltaf, E. Durgun, J.-Y. Raty, Ph. Ghosez, and X. Gonze, Phys. Rev. B **78**, 205203 (2008); R. Shaltaf, X. Gonze, M. Cardona, R. K. Kremer, and G. Siegle, *ibid.* **79**, 075204 (2009).

[7] M. J. Polking, J. J. Urban, D. J. Milliron, H. Zheng, E. Chan, M. A. Caldwell, S. Raoux, C. F. Kisielowski, J. W. Ager, III, R. Ramesh, and A. P. Alivisatos, Nano Lett. **11**, 1147 (2011).

[8] P. Fons, A. V. Kolobov, M. Krbal, J. Tominaga, K. S. Andrikopoulos, S. N. Yannopoulos, G. A. Voyiatzis, and T. Uruga, Phys. Rev. B **82**, 155209 (2010).

[9] T. Matsunaga, P. Fons, A. V. Kolobov, J. Tominaga, and N. Yamada, Appl. Phys. Lett. **99**, 231907 (2011).

[10] R. E. Peierls, *Quantum Theory of Solids* (Oxford University Press, New York, 2001).

[11] J. N. Bierly, L. Muldawer, and O. Beckman, Acta Metall. **11**, 447 (1963); H. Wiedemeier and P. A. Siemers, Z. Anorg. Allg. Chem. **431**, 299 (2004); E. M. Levin, M. F. Besser, and R. Hanus, J. Appl. Phys. **114**, 083713 (2013).

[12] R. Tsu, W. E. Howard, and L. Esaki, Phys. Rev. **172**, 779 (1968); Solid State Commun. **5**, 167 (1967).

[13] S. K. Bahl and K. L. Chopra, J. Appl. Phys. **40**, 4940 (1969); J. E. Lewis, Phys. Status Solidi B **59**, 367 (1973).

[14] J. E. Lewis, Phys. Status Solidi B **35**, 737 (1969); S. K. Bahl and K. L. Chopra, J. Appl. Phys. **41**, 2196 (1970).

[15] F. Tong, X. S. Miao, Y. Wu, Z. P. Chen, H. Tong, and X. M. Cheng, Appl. Phys. Lett. **97**, 261904 (2010); E. M. Levin, M. F. Besser, and R. Hanus, J. Appl. Phys. **114**, 083713 (2013).

[16] J. M. Leger and A. M. Redon, J. Phys.: Condens. Matter **2**, 5655 (1990); A. Onodera, I. Sakamoto, Y. Fujii, N. Môri, and S. Sugai, Phys. Rev. B **56**, 7935 (1997).

[17] P. Bauer Pereira, I. Sergueev, S. Gorsse, J. Dadda, E. Müller, and R. P. Hermann, Phys. Status Solidi B **250**, 1300 (2012).

[18] J. J. Gervacio-Arciniega, E. Prokhorov, F. J. Espinoza-Beltrán, and G. Trapaga, J. Appl. Phys. **112**, 052018 (2012).

[19] F. Kadlec, C. Kadlec, P. Kužel, and J. Petzelt, Phys. Rev. B **84**, 205209 (2011).

[20] K. M. Rabe and J. D. Joannopoulos, Phys. Rev. B **36**, 3319 (1987).

[21] U. V. Waghmare, N. A. Spaldin, H. C. Kandpal, and R. Seshadri, Phys. Rev. B **67**, 125111 (2003).

[22] A. H. Edwards, A. C. Pineda, P. A. Schultz, M. G. Martin, A. P. Thompson, H. P. Hjalmarson, and C. J. Umrigar, Phys. Rev. B **73**, 045210 (2006).

[23] H. Mutka, Physica B **180–181**, 929 (1992).

[24] H. Schober, A. Tölle, B. Renker, R. Heid, and F. Gompf, Phys. Rev. B **56**, 5937 (1997).

[25] S. W. Lovesey, *Theory of Neutron Scattering from Condensed Matter* (Oxford University Press, New York, 1987); G. L. Squires, *Introduction to the Theory of Thermal Neutron Scattering* (Cambridge University Press, Cambridge, 1978).

[26] U. D. Wdowik, K. Parlinski, T. Chatterji, S. Rols, and H. Schober, Phys. Rev. B **82**, 104301 (2010).

[27] J. Rodríguez-Carvajal, Physica B **192**, 55 (1993).

[28] G. Kresse and J. Furthmüller, Phys. Rev. B **54**, 11169 (1996); Comput. Mater. Sci. **6**, 15 (1996).

[29] J. P. Perdew, K. Burke, and M. Ernzerhof, Phys. Rev. Lett. **77**, 3865 (1996); **78**, 1396 (1997).

[30] P. E. Blöchl, Phys. Rev. B **50**, 17953 (1994); G. Kresse and D. Joubert, *ibid.* **59**, 1758 (1999).

[31] K. Parlinski, Z. Q. Li, and Y. Kawazoe, Phys. Rev. Lett. **78**, 4063 (1997); K. Parlinski, software PHONON ver. 6.14 (Krakow, Poland, 2013).

[32] R. M. Pick, M. H. Cohen, and R. M. Martin, Phys. Rev. B **1**, 910 (1970).

[33] M. Gajdoš, K. Hummer, G. Kresse, J. Furthmüller, and F. Bechstedt, Phys. Rev. B **73**, 045112 (2006).

[34] P. Umari, A. Pasquarello, and A. Dal Corso, Phys. Rev. B **63**, 094305 (2001); P. Umari, X. Gonze, and A. Pasquarello, Phys. Rev. Lett. **90**, 027401 (2003); M. Ceriotti, F. Pietrucci, and M. Bernasconi, Phys. Rev. B **73**, 104304 (2006).

[35] K. Parlinski, Z. Q. Li, and Y. Kawazoe, Phys. Rev. B **61**, 272 (2000).

[36] H. T. Stokes and D. M. Hatch, *Isotropy Subgroups of the 230 Crystallographic Space Groups* (World Scientific, Singapore, 1988).

[37] K. Parlinski and Y. Kawazoe, Eur. Phys. J. B **16**, 49 (2000).

[38] K. Parlinski, Y. Kawazoe, and Y. Waseda, J. Chem. Phys. **114**, 2395 (2001).

[39] D. M. Hatch and H. T. Stokes, J. Appl. Cryst. **35**, 379 (2002); Phys. Rev. B **65**, 014113 (2001).

[40] The $Fm\bar{3}m \rightleftharpoons R3m$ transition driven by the triply degenerate soft Γ_4^- phonon proceeds without a change in size of the primitive unit cell while going from the parent to the daughter phase.

[41] J.-P. Gaspard, A. Pellegatti, F. Marinelli, and C. Bichara, Philos. Mag. B **77**, 727 (1998); J. Y. Raty, V. Godlevsky, P. Ghosez, C. Bichara, J. P. Gaspard, and J. R. Chelikowsky, Phys. Rev. Lett. **85**, 1950 (2000); J. Akola and R. O. Jones, Phys. Rev. B **76**, 235201 (2007); P. Silas, J. R. Yates, and P. D. Haynes, *ibid.* **78**, 174101 (2008).

[42] G. Henkelman, A. Arnaldsson, and H. Jónsson, Comput. Mater. Sci. **36**, 354 (2006); W. Tang, E. Sanville, and G. Henkelman, J. Phys.: Condens. Matter **21**, 084204 (2009).

[43] The rocksalt $Ge_{1-x}Te$ with $x = 1\%$ is also metallic.

[44] T. Schneider and E. Stoll, Phys. Rev. B **13**, 1216 (1976).